

Melt in the Greenland EastGRIP ice core reveals Holocene warm events

Julien Westhoff¹, Giulia Sinnl¹, Anders Svensson¹, Johannes Freitag², Helle Astrid Kjær¹, Paul Vallelonga¹, Bo Vinther¹, Sepp Kipfstuhl², Dorthe Dahl-Jensen^{1,3}, and Ilka Weikusat^{2,4}

¹Niels Bohr Institute, University of Copenhagen, Copenhagen, Denmark

²Alfred-Wegener-Institut Helmholtz-Zentrum für Polar- und Meeresforschung, Bremerhaven, Germany

³Centre for Earth Observation Science, University of Manitoba, Canada

⁴Department of Geosciences, Eberhard Karls University Tübingen, Germany

Correspondence: Julien Westhoff (julien.westhoff@nbi.ku.dk)

Abstract.

We present a record of melt events obtained from the East Greenland Ice Core Project (EastGRIP) ice core, in central northeastern Greenland, covering the largest part of the Holocene. The data were acquired visually using an optical dark-field line scanner. We detect and describe melt layers and -lenses, seen as bubble-free layers and -lenses, throughout the ice above the bubble-clathrate transition. This transition is located at 1150 m depth in the EastGRIP ice core, corresponding to an age of 9720 years b2k. We define the brittle zone in the EastGRIP ice core from 650 m to 950 m depth, where we count on average more than three core breaks per meter. We analyze melt layer thicknesses, correct for ice thinning, and account for missing layers due to core breaks. Our record of melt events shows a large, distinct peak around 1014 years b2k (986 CE) and a broad peak around 7000 years b2k corresponding to the Holocene Climatic Optimum. In total, we can identify approximately 831 mm of melt (corrected for thinning) over the past 10,000 years. We find that the melt event from 986 CE is most likely a large rain event, similar to 2012 CE and that these two events are unprecedented throughout the Holocene. We also compare the most recent 2500 years to a tree ring composite and find an overlap between melt events and tree ring anomalies indicating warm summers. Considering the ice dynamics of the EastGRIP site resulting from the flow of the Northeast Greenland Ice Stream (NEGIS), we find that summer temperatures must have been at least 3 ± 0.6 °C warmer during the Early Holocene compared to today.

1 Introduction

1.1 What are melt layers?

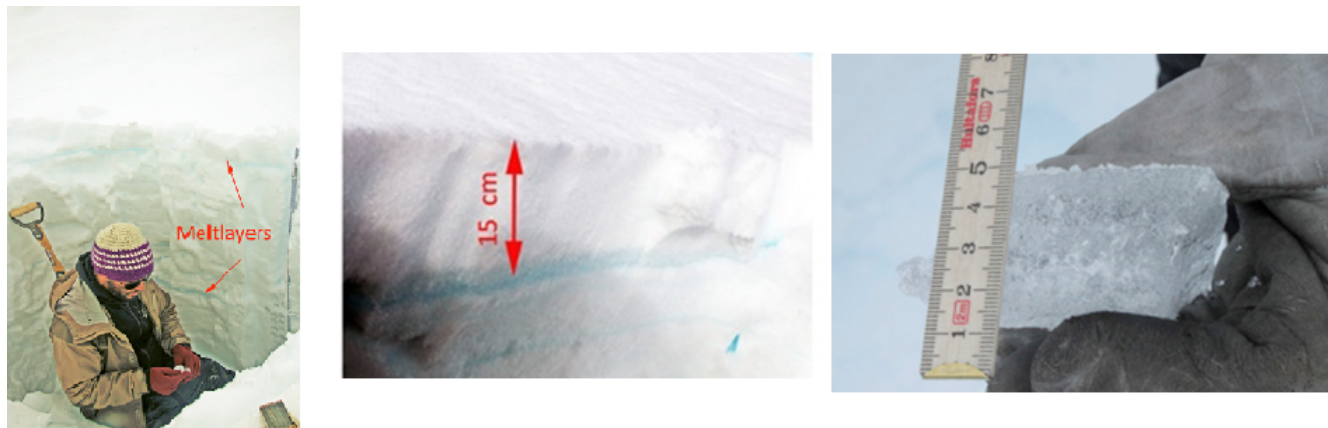


Figure 1. a) View into the snowpit dug just after the 2012-rain/melt event at NEEM. The resulting melt layers occur in depths of around 15 and 70 cm below surface. b) close up on the upper melt layer and c) the 3.5 centimeter thick layer.

Melt layers are commonly thought of as events with surface melt due to intense solar radiation and/or high temperature leading to the formation of superficial liquid melt puddles followed by their percolation into the snowpack (e.g. Shoji and Langway, 1987; Humphrey et al., 2012). Thick clouds bringing in high air temperatures, possibly enhanced by local albedo changes due to dark particles (Keegan et al., 2014), have triggered the 1889 and 2012 CE melt events across Greenland, which are the two largest melt events in recent history (e.g. Nghiem et al., 2012; Bonne et al., 2015). Another possible cause for enhanced surface melting is a reduction of the snow albedo, from a previous melt layer close to the surface, which is still exposed due to the lack of further precipitation (Keegan et al., 2014). Occurring less frequently, rain events over an ice sheet can lead to the same type of features.

The features in the snowpack resulting from superficial melt water can be distinguished into: horizontal melt layers and lenses (Das and Alley, 2005), and vertical melt pipes (Pfeffer and Humphrey, 1998). These features stand out in the stratigraphy as they are bubble-free (more details in the methods section). It is also possible for water to refreeze homogeneously throughout a section of the snow pack, in the absence of a low-permeability layer.

1.2 Greenland melt layer records

A 10,000 year melt layer record from a Greenlandic ice core was presented by Alley and Anandakrishnan (1995) on the Greenland Ice Sheet Project 2 (GISP2) ice core, who applied visual inspection during ice core processing. Herron et al. (1981) also use visual inspection on the DYE3 ice core from southern Greenland, to create a 2200 year melt record. Similar visual methods, in addition to density measurements, were used by Freitag et al. (2014 EGU poster) on two shallow cores around

35 DYE3 and South Dome in Greenland. Shorter melt records have been established at other southern Greenland sites, such as site A (70,8 °N, 36,0 °W, 3145 m, Alley and Koci, 1988), site J (66°51.9'N, 46°15.9'W, 2030 m, Kameda et al., 1995) or in Western Greenland (Trusel et al., 2018).

A range of techniques have been applied to investigate melt layers in ice cores from Greenland and other locations: Keegan et al. (2014) compared multiple shallow cores across the dry snow zone in Greenland and show a spatial variability of melt layers, with only the warm summer event from 1889 CE being visible in all cores (cores were drilled before 2012 CE).

Studies of melt features in the ablation zone of the Greenland ice sheet have been conducted using multiple shallow ice cores (e.g. Graeter et al., 2018), or snow pits (e.g. Humphrey et al., 2012). Combined computer tomography (CT, Schaller et al., 2016) and visual analysis using line scan images (see methods section) for melt layer detection was applied on the Renland Ice Cap (RECAP) ice core, coastal eastern Greenland, by Taranczewski et al. (2019), combining one deep and two shallow cores. Melt layer records have been established for many glaciated sites around the world, e.g. in Canada (Koerner and Fisher, 1990; Fisher et al., 1995; Fisher et al., 2012), Alaska (Winski et al., 2018), and Arctic Russia (Fritzsche et al., 2005).

Melt, or bubble-free, layer records for the past 10,000 years have only been identified for the GISP2 (Alley and Anandakrishnan, 1995) and the RECAP (Taranczewski et al., 2019) ice cores. In deep ice cores, such as GISP2, bubbles transform to clathrates and become difficult to detect visually (Kipfstuhl et al., 2001). Methods to detect melt layers from clathrate distributions have not succeeded yet. In the RECAP ice core, the Holocene ice covers 533 of a total core length of 584 meters (Simonsen et al., 2019). Here the stratigraphy of the deepest layers of the Holocene (Early Holocene) are thinned too much to detect single melt layers. Therefore, all analysis to date are limited to the past 10,000 years, with the exception of NEEM community members (2013) and Orsi et al. (2015), who investigated noble gas (isotopes) to detect melt layers on selected samples of Eemian section of the North Greenland Eemian Ice Drilling (NEEM) ice core.

More common methods to detect melt layers are identifying irregularities in the Electronic Conductivity Measurements (ECM, pers. comm. Sune Rasmussen), or anomalies in stable water isotope records (Valerie Morris, in prep.). More recent melt events can be detected using satellite images: as an example Steen-Larsen et al. (2011) describe six recent melt events at the NEEM site. Combining satellite and ice core data to create a melt archive is done in several studies such as Mote (2007), Keegan et al. (2014), or Trusel et al. (2018). Melt layers, i.e. bubble-free layers, can easily be confused with wind crusts (see method section), that are studied by Fegyveresi et al. (2018) and Weinhart et al. (2021).

1.3 In-situ analysis of the 2012 CE melt and rain event

The 2012 CE melt and rain event in Greenland is very well observed and documented, e.g. Nghiem et al. (2012), Tedesco et al. (2013), Nilsson et al. (2015), or Bonne et al. (2015). Bonne et al. (2015) provide a detailed study on the atmospheric conditions leading to the rain event, in combination with field observations, e.g. from Steen-Larsen et al. (2011). Nilsson et al. (2015) present a detailed study on the 2012 CE melt event using CryoSat-2 radar altimetry. Polar ice sheets are colder under clear-sky conditions, as snow absorbs and radiates effectively in the longwave but reflects in the shortwave. Eye witnesses from NEEM, DYE3, and South Dome in Greenland verify that thick clouds brought in the high air temperatures which lead to the 2012 CE warm event across Greenland. Observations at the NEEM drill site show that the surface temperature exceeded the

melting point over five days, and that melt layers formed at approximately 5, 20, and 69 cm depth (Nghiem et al., 2012). In the supplement, we include an overview of the temperature evolution of the snowpack during the 2012 CE warm event. Using the words of Trusel et al. (2018): “For the most recent 350 years in Greenland ice core, 2012 melt is unambiguously the strongest melt season on record.”

A problem with interpreting melt layers is shown in the snowpit sampling during the 2012 CE melt event at NEEM (fig. 1 and fig. A1c). When a melt event creates multiple melt layers, the uppermost melt layers remain in the snow of that year and the lower ones may percolate into snow from the previous years. This is also true for melt events which only form one layer, yet larger melt events seem to percolate deeper into the snowpack.

In the supplement, we also present the result from a simple rain-melt-event-experiment performed in April 1995, using cold coffee as a colored substitute for melt (fig. A1a,b). In a more recent study, Pfeffer and Humphrey (1998) perform a very detailed analysis on melt water infiltration into the snowpack. Therefore, interpretations of melt events on an annual time scale should be handled with care, and the uppermost layer should be taken as a reference. This effect can be neglected on the decadal and lower temporal resolution.

1.4 Climate of the Holocene

Melt layers can be found in ice cores throughout the Holocene in central Greenland. To analyze and understand these, a climatic overview is necessary: Axford et al. (2021) have compiled different records of the Holocene climate in Greenland (fig. 2), including the GISP2 melt layer record (Alley and Anandakrishnan, 1995). Their study offers two possible climatic reconstructions: A climatic optimum around the Early Holocene, as shown by pollen, geological records, and $\delta^{15}N$ from ice cores (e.g. fig. 2c), or a damped climatic optimum, as shown by the $\delta^{18}O$ from ice cores (fig. 2d). The dampening of these warm temperatures during the Early Holocene, is due to a larger ice sheet with higher surface elevation (fig. 2a,h), and therefore cooler temperatures, from ice core reconstructions, due to a higher lapse rate (e.g. Brunt, 1933; Gardner et al., 2009; Vinther et al., 2009).

The timing and intensity of the Holocene Climatic Optimum (HCO) is still debated: e.g. Lecavalier et al. (2017) find an early and intense HCO, while e.g. Badgeley et al. (2020) argue for a later HCO. Bova et al. (2021) argue that the warm temperatures at the beginning of the Holocene are a bias caused by proxies mostly affected by warmer summer temperatures (fig. 2g), and larger seasonal variations, while the annual mean temperature remained lower and gradually climbed to today’s value more or less following atmospheric CO_2 concentrations (fig. 2f).

1.5 The EastGRIP site

The East Greenland Ice Core Project (EastGRIP) ice core, on which we create our melt layer record, is drilled through the Northeast Greenland Ice Stream (NEGIS, fig. 2a). This ice stream flows from the ice divide, between NorthGRIP and the summit area, towards the NNE until it terminates at the coast (Vallelonga et al., 2014). Today’s position of the EastGRIP drill site moves with approximately 55 m/yr (Hvidberg et al., 2020), i.e. approximately 15 cm per day.

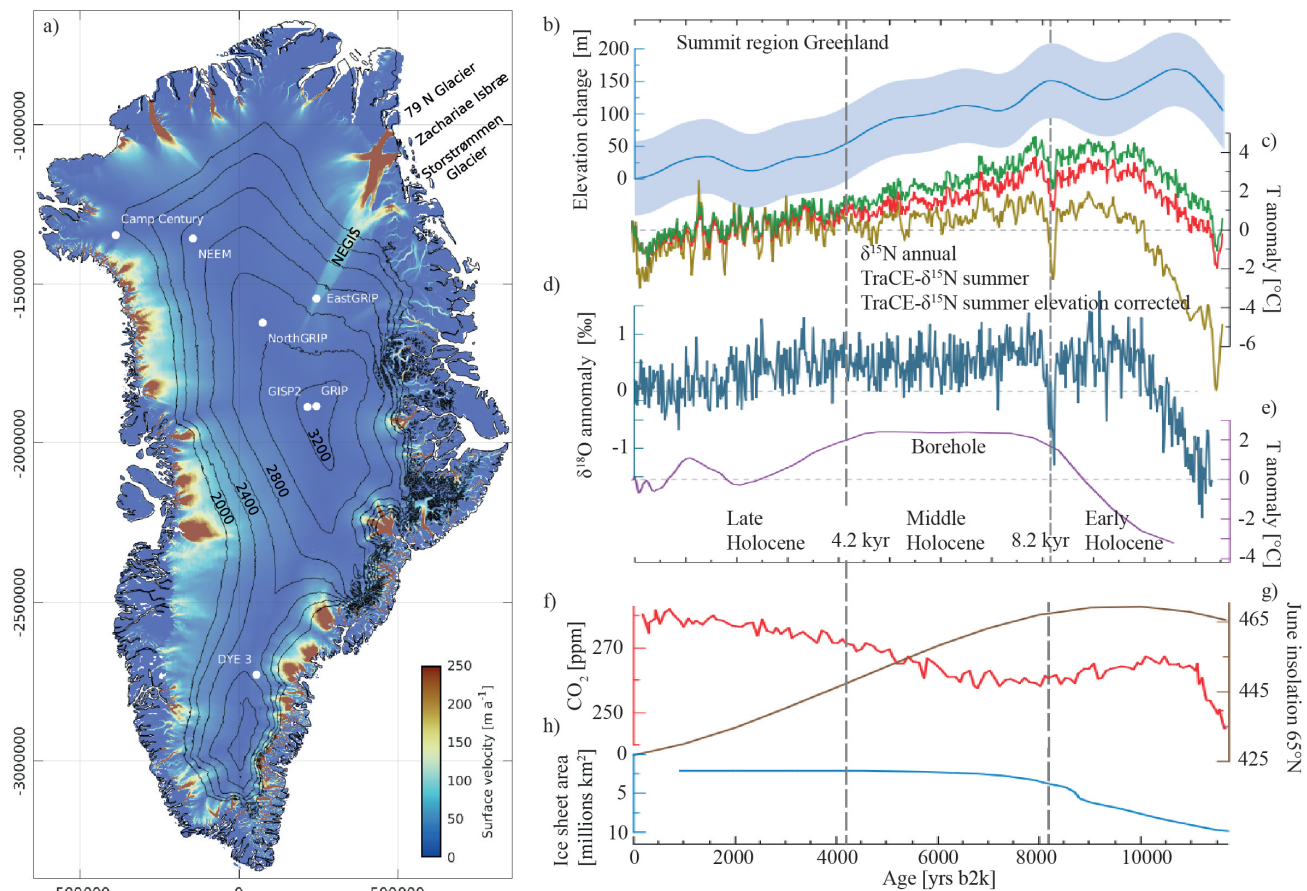


Figure 2. a) Overview map of Greenland, including relevant ice core drill sites and surface velocities from Gerber et al. (2021). b) to h) Modified from Axford et al. (2021, fig. 2 and 3e). The vertical dashed lines mark the boundary between Early and Middle, and Middle and Late Holocene at 8.2 kyr and 4.2 kyr, respectively. All proxies are shown as anomalies relative to the 1930–1970. b) Estimated surface elevation change at Summit (dark blue, Vinther et al., 2009) and uncertainty (faded blue shading, Lecavalier et al., 2013), c) annual $\delta^{15}N$ (dark yellow) and summer (red) and elevation-corrected summer (green) Summit temperature anomalies from TraCE- $\delta^{15}N$ (Buizert et al., 2018), d) GRIP oxygen isotopes (Rasmussen et al., 2006; Vinther et al., 2006), e) GRIP borehole temperature reconstruction (Dahl-Jensen et al., 1998), f) atmospheric CO_2 (Monnin et al., 2004), g) Climate forcings and influences including June insolation (Berger and Loutre, 1991), and h) decline of the Laurentide-Innuitian-Cordilleran ice sheet complex (Dalton et al., 2020), y-axis reversed.

2 Methods

2.1 Depth of interest

Our analysis covers the upper 1090 m of the EastGRIP ice core, corresponding to the years 1965 CE to 7604 BCE, i.e. 9569 years. We use the age scale provided by Mojtabavi et al. (2020) and the time reference “years before the year 2000 CE” (yrs
105 b2k).

The depth notation in this work refers to the depth below the 2017 ice sheet surface, the year in which ice core drilling began. Ice core processing started 13.75 m below the surface, which corresponds to the year 1965 CE (44 yrs b2k, Mojtabavi et al., 2020). Thus, this is the youngest material available for our analysis.

We terminate our investigation of bubble-free layers at a depth of 1090 m, approximately 9604 yr b2k, because of the almost
110 complete transition from air bubbles to clathrates (e.g. Shoji and Langway, 1987; Kipfstuhl et al., 2001; Uchida et al., 2014). With bubbles becoming smaller and eventually transforming to clathrates under increasing pressure, the spacing between bubbles increases, and bubble-free layers become increasingly difficult to identify. This bubble-clathrate transformation is not a gradual process over depth, but has variable rates for different layers due to their physical properties and the resulting complex crystallization of air hydrates (Weikusat et al., 2015). We use the line scan images (next section) to find that the conversion
115 from bubbles to clathrates is fully completed in a depth of 1150 m, but end our analysis 60 m above that depth.

2.2 The line scanner and its images

The line scanner is a well-established and powerful tool for high resolution analysis of ice stratigraphy, making use of contrast enhancement by the optical dark-field method (Faria et al., 2018). Different devices with similar setups have been used on many deep ice core since the NorthGRIP drilling in 1995 (e.g. Svensson et al., 2005; McGwire et al., 2008; Jansen et al.,
120 2016; Faria et al., 2018; Morcillo et al., 2020; Westhoff et al., 2020). The device used at EastGRIP is the second generation Alfred-Wegener-Institute (AWI) line scanner. Images are obtained with a camera moving along the top of a 165 cm long and 3.6 cm thick ice core slab (Weikusat et al., 2020). Two light sources illuminate the polished ice core slab at an angle from below (for details consult Svensson et al., 2005; Westhoff et al., 2020).

The appearance of line scan images is substantially different from firn to ice (fig. 3 left and right, respectively). In firn and
125 snow, the bright sections of the image represent the solid parts, such as snow crystals, firn grains, or ice layers. The high number of firn grains, and thus many grain boundaries, reflect the light causing the bright appearance. Dark sections of the image represent voids, i.e. air. When firn has been compressed to ice, the appearance of features is inverted: ice now appears dark and bubbles, i.e. air, are now represented by bright pixels. In ice the open pores and voids between single grains have been closed, which allows light to travel through without any reflections, thus a dark field below the ice core slab is imaged. Bubbles
130 appear bright, as their rounded ice-air interface offers perfect conditions for light scattering in all directions.

At EastGRIP, the firn-ice transition is situated at around 70 m depth (e.g. Buizert et al., 2012), so the largest part of our investigation is conducted on ice with bubbles, where bubble-free layers are easy to identify (e.g. fig. 3d).

2.3 Types of events

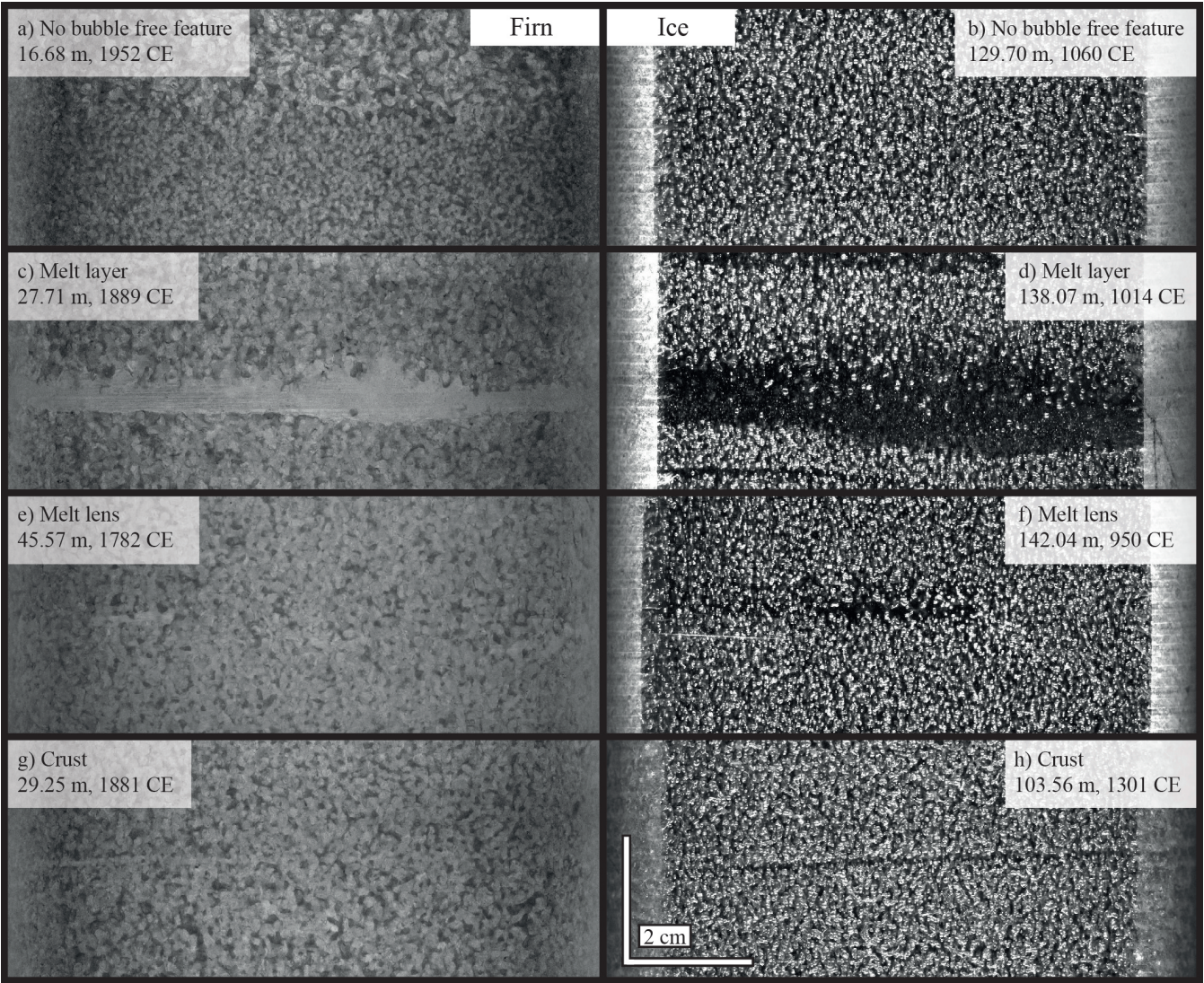


Figure 3. The appearance of different structures in line scan images in firn (left) and ice (right). a,b) Typical examples of appearance of firn and ice. c,d) bubble-free layers interpreted as melt layers. These are continuous horizontally across the ice core. e,f) bubble-free lenses interpreted as melt lenses, which are discontinuous patches mostly with a horizontal elongation. g,h) Very thin and straight bubble-free layers with sharp edges. These structures are hard to see in line scan images and are interpreted as crusts, the result of surface hardening by the wind.

In the upper 1100 m of the EastGRIP ice core the majority of the ice contains bubbles, and thus the “normal” appearance
135 of firn and ice (fig. 3a,b). Firn and ice can be bubble-free for two reasons: either snow melted and refroze close to the surface,

creating a melt layer or lens, or a surface hardening took place e.g. by wind which forms hard (wind-)crusts. On this basis we define three types of bubble-free features: melt layers (fig. 3c,d), melt lenses (fig. 3e,f), and crusts (fig. 3g,h). Within our three categories, we note the certainty of our labeling as either “certain” or “uncertain”. The process of data acquisition and depth registration can be found in the supplement.

140 We define the different types as follows:

- Melt layers are in general continuous features ranging across the entire horizontal core width (10 cm). The melt layer thickness can vary within one layer, but we define, that it should always be greater than one millimeter at its narrowest point ($1\text{ mm} = 18.6\text{ pixels}$). They can have sharp edges (fig. 3c bottom left) or smooth edges, where bubbles are within the melt layer (fig. 3d top edge).
- 145 – Melt lenses have the same appearance as melt layers, yet are of smaller dimensions and not continuous across the width of the core. The definition of layer and lens is therefore determined by the core diameter, which in the EastGRIP ice core is approximately 10 cm. Lenses can have a rounded shape, yet in general, they show an elongation along the horizontal. These disk shape structures point to a melt layer above and to not over estimate the number of events, the lens itself should thus not be seen as a separate event (pers. comm. Sepp Kipfstuhl).
- 150 – Crusts are very thin bubble-free layers, around one millimeter, and in general continuous from one side of the core to the other. They have a sharp border to the bubbles around them. These thin layers can be identified reasonably well and distinguished from melt layers in the upper 250 m. Yet as thinning of layers proceeds, a distinction is no longer possible from the 2D line scan images. We therefore assume that below 250 m, all layers with the appearance of crusts are actually thinned melt layers. Thinning would be influential to such a degree that crusts are eventually no longer detectable using
- 155 line scan images.

2.4 Core breaks and the brittle zone

Core breaks influence the counting of melt layers and lenses. Core breaks are fractures in the core, mainly occurring for two reasons: either from breaking the ice core free at the bottom of the borehole (see Westhoff et al., 2020), or from fractures in the brittle-zone ice (Neff, 2014).

- 160 – The drilling-related core-breaks are usually approximately horizontal. During smooth drilling operations and good ice quality, core breaks occur every few meters, depending on the length of the core barrel chamber which is implemented in the deployed drilling system.
- In the brittle zone, where the internal pressure of the trapped air bubbles is very high and exceeds the tensile strength of the ice core, the ice core samples will break up and sometimes even explode. This is an effect of pressure-temperature relaxation after core recovery at the surface. Core breaks in the brittle zone could have any orientation and thus tend to
- 165 run diagonally across the core and line scan image.

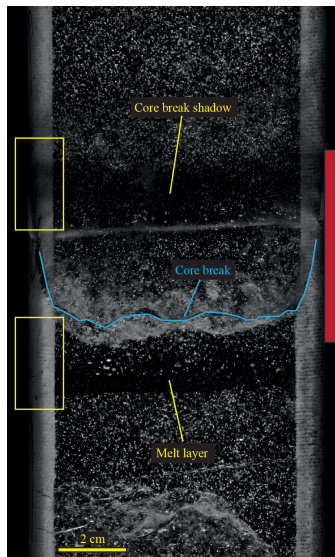


Figure 4. A core break casting a shadow and a melt layer have a very similar appearance in the line scan images. A distinction is made first by the proximity to the break, and then by differences of brightness along the ice core’s round drilling edge (yellow boxes). Core break shadows darken the edge of a sample. Minimum section not suited for analysis is indicated by red bar.

During line scanning, light is introduced at an angle from below the core slab. As core breaks usually have a rough break-surface, followed by a gap and another rough break-surface, the light intensity will drop when crossing the void. This intensity loss casts shadows on either side of the core breaks. These shadows greatly depend on the geometry of the core break and can easily be mistaken for a bubble-free layer. A rare occasion (one of two in total) is fig. 4, where a melt layer is very close to a break. The core break is distinguishable from a melt layer, because the core break casts a shadow on the edge of the core slab, while the edge remains at a constant brightness in the presence of a melt layer (yellow boxes in fig. 4). Similar to the core break shadows are the saw-cut shadows, which appear at the ends of each 165 cm-long line scan.

To account for this difficulty, features close to core breaks and the edge of the images are in general disregarded. This implies, that the more core breaks we have, the more bubble-free events we may miss and the more we underestimate the number of events. It is, therefore, necessary to obtain an overview of core breaks throughout the depth of interest. We estimate the chance of missing a bubble-free event by assuming a 4 cm-sample loss for each break. In general, a shadow is cast 1.5 cm to either side of the break and the break itself disturbs the image across at least 1 cm, adding up to 4 cm in total (fig. 4, red bar).

2.5 Northern hemisphere tree rings

Sigl et al. (2015) created a Northern Hemisphere temperature reconstruction using the tree ring composite record (N-Tree), which we compare to melt events. The tree ring record comprises tree ring growth anomalies from five different locations across the Northern Hemisphere, where temperature is the limiting factor to growth. The N-Tree record is presented on its independent annual ring-width timescale (NS1-2011), carrying no uncertainty according to Sigl et al. (2015). The individual

records from northern locations in Finland, Sweden, Siberia, Central Europe, and USA almost always overlap, providing a
185 composite average of the tree growth in response to temperature.

For the comparison of melt events to the tree ring data, we translate the EastGRIP (Greenland Ice Core Chronology 2005: GICC05) ages to the tree ring timescale (NS1-2011). We verified good alignment of EastGRIP and N-Tree data as many volcanic eruptions align to drastic cooling events within one to two years. We refer to ages and events using the GICC05 timescale, for consistency throughout the manuscript.

3.1 Melt events

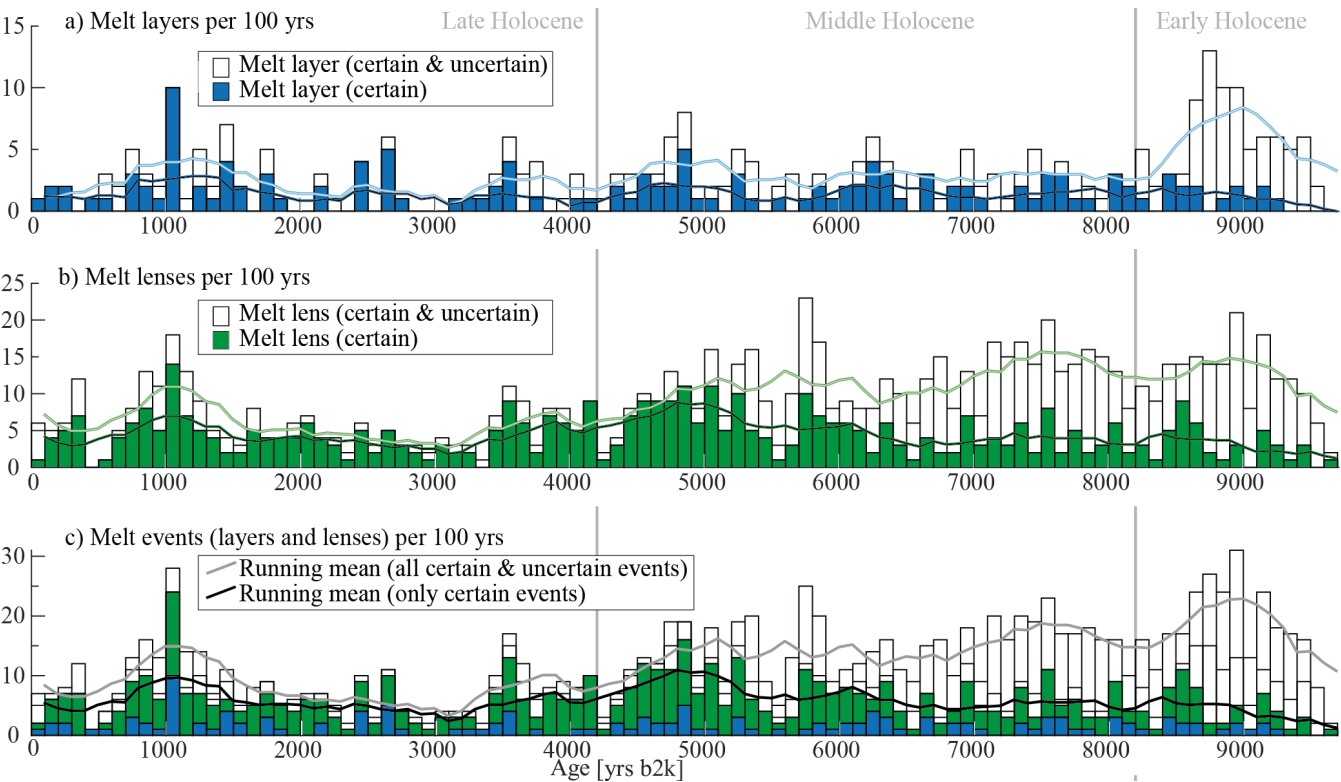


Figure 5. Number of melt layers and lenses per century throughout the last 9700 years in the EastGRIP ice core. Running means are shown as solid lines. a) Melt layers (dark blue) and uncertain melt layers (white), b) melt lenses (dark green) and uncertain melt lenses (white), c) melt events, i.e., stack of panels a) and b), including their uncertainties. Note that the bar representing the period from 0 to 100 yrs b2k only represents 56 years, and not 100 like the other bars, as our analysis only begins in 1956 CE.

We find 561 melt events throughout the last 9700 years in the EastGRIP record (fig. 5c), which can be separated into 137 melt layers (fig. 5a) and 424 melt lenses (fig. 5b). Melt lenses are thus almost three times more frequent and represent smaller events. We find another 622 uncertain events, of which 157 are uncertain melt layers and 465 uncertain melt lenses (fig. A2).

195 Both melt lenses and layers follow the same trend and are most abundant during the same periods. As both features represent refrozen melt water, we can consequently group them together as melt events (fig. 5). For events we are certain of, we see a gradual decrease in number of events towards the Early Holocene. We find very few or no melt layers around the years 500, 2000, and 3000 b2k, and also melt lenses are less frequent. We find many certain melt events (dark blue and dark green in fig. 5), around the years 1000, 3500 to 4000, 4500 to 5200, and around 6000 b2k. We then continuously find melt events in
200 between 6000 and 9000 yrs b2k, yet in varying number.

Including uncertain events, the number of events shows a slight increase towards the Early Holocene. These are melt layers and lenses that are difficult to see in the line scan data, and should thus be treated with caution.

Events older than 9000 years become difficult to detect due to progressive bubble to clathrate transformation, therefore values gradually decrease. Slightly before 9000 yrs b2k the ratio of uncertain to certain layers increases, indicating the difficulty in
205 detecting melt layers. Also, we do not capture the most recent years, younger than 44 yrs b2k (1956 CE).

3.2 Core breaks and their implications

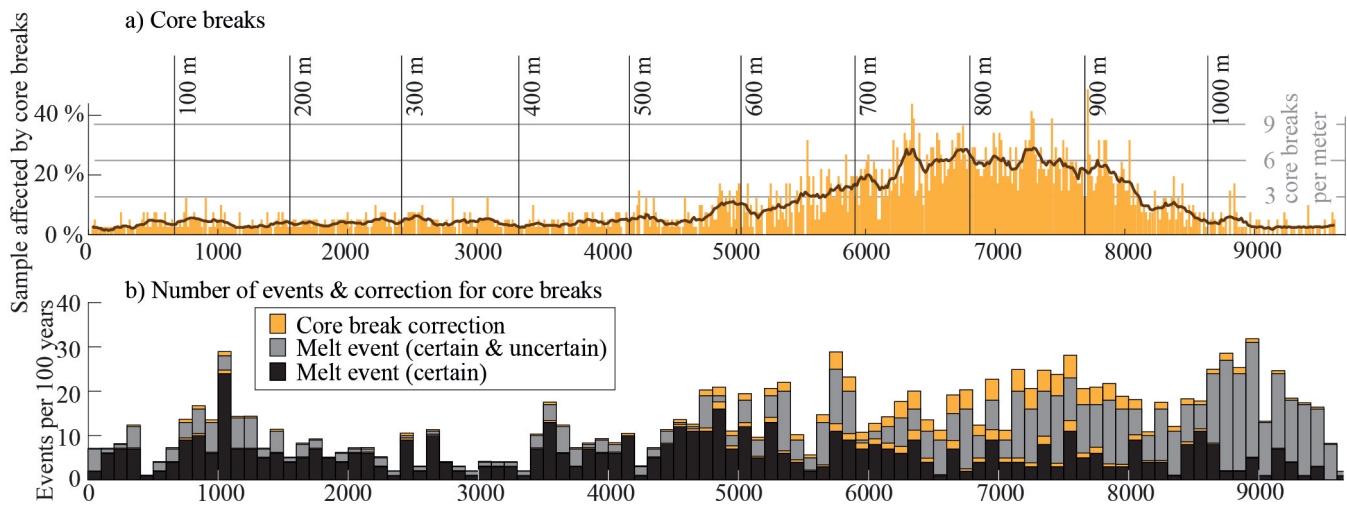


Figure 6. a) Percentage of 165 cm-sample affected by core breaks (orange bars, scale left side), amount of core breaks per meter (orange bars, scale right side), and running mean over 16.5 meters (brown line). The broad peak between 650 and 950 m depth indicates the brittle zone. b) Certain melt events (black) and uncertain melt events (gray) corrected for potentially missed events in proximity of core breaks (orange).

We count core breaks (fig. 6a, orange bars) in the upper 1100 m of the EastGRIP ice core and show the corresponding ages and depths. The running mean over 16.5 meters (fig. 6a, brown line) clearly locates the brittle zone between 650 and 950 m depth. In the brittle zone, the number of core breaks greatly increases and exceeds three breaks per meter (or five breaks per
210 165-cm sample). As a core break masks four centimeters, we lose almost 25% of the sample in sections with six core breaks per meter.

As we know the number of melt events per sample, we can estimate the number of events missed due to core break shadows (fig. 4). Events per 100 years are shown by vertical bars and the potentially missed melt events, i.e. our core break correction, in orange (fig. 6b). The largest corrections are therefore performed in the brittle zone where we add around 25% to the number
215 of melt events. This does not change the overall picture much but shows that we probably underestimate melt events in the time between 6000 and 8000 yrs b2k.

Our correction described above, assumes no correlation between the location of core breaks and melt layers. This correlation could be expected as melt layers might affect the crystal structure or other physical properties of the core. We perform a non quantitative visual inspection and do not find any connection of melt layers weakening or strengthening the ice and thus affecting the initiation and location of core breaks in the brittle zone.

3.3 Melt layer thickness and total melt

For the 137 certain melt layers, we have documented their thickness (M_0 , fig. 7). Melt lenses are excluded from this analysis, as their average thickness is below one millimeter, and has not been measured. The layer thickness of melt layers is shown by the yellow, orange, and red bars, and to distinguish events within a short period, the thickness is indicated by circles. Cases of multiple events within five years are marked with a star (fig. 7c). We find three cases with three or more events within five years (red star) and 13 cases with two layers in five years (blue star).

We correct the melt layer thickness for thinning (initial thickness, M_0 , open circles to corrected thickness, M , filled circles, fig. 7a,b,c), using the thinning function from Gerber et al. (2021, fig. 7d). Here we must keep in mind that the thinning is an average over tens of meters, derived from radar data. It is thus an upper limit assumption for the thinning of melt layers, which are denser, due to the lack of bubbles, and should therefore thin less than the surrounding ice.

Thin melt layers ($M < 4mm$, yellow) are found throughout the Holocene, yet seem to be more abundant in the Late Holocene (last 4200 years before today). Thick melt layers ($M > 8mm$, red) become more frequent further back in time (positive trend blue line in fig. 7b). The thinning-corrected running mean (solid blue line, fig. 7b,c) points to an average melt layer thickness of around 5 mm for the past 4500 years. Going back further in time, we see a gradual increase in melt layer thickness in ice older than 4500 years (fig. 7c), peaking at an average thickness of 8 mm around 6500 to 7000 yrs b2k (solid blue line). In events older than 7000 years, the mean gradually drops. We find the last melt layer in ice deposited 9235 yrs b2k.

We expect to miss thinner melt layers the further back we go in time, which is represented by our results (fig. 7c) where we only find seven thin melt layers ($M < 4mm$, yellow) between 7000 and 9700 yrs b2k. In the same period we find 15 medium ($4mm < M < 8mm$, orange) and nine thick melt layers ($M > 8mm$, red). Assuming we miss thin layers but not thicker ones, we would expect a continuous increase in average melt layer thickness. Yet this average (blue line, fig. 7c) gradually drops below 7500 yrs while we approach Holocene Climatic Optimum (HCO). A possible reason for this gradual drop could be the two cooling events 8200 and 9300 years ago (Alley et al., 1997; Thomas et al., 2007; Rasmussen et al., 2007).

We only find melt layers exceeding a thickness of 15 mm between 6100 and 8100 yrs b2k, with one exception at 1014 yrs b2k (fig. 7c). This allocates the majority of thick melt layers to the Middle Holocene (Northgrippian Period, Cohen et al., 2016). An overview of thickness distributions can be found in fig. A3.

Derived from melt layer thicknesses, we present a melt layer record of the total amount of melt per century and millenium (fig. 7e,f, respectively). This record is corrected for thinning, using values from fig. 7c and we account for potentially missed layers due to core breaks (orange, from fig. 6). Layers thinner than 1.54 mm have been removed for consistency (see fig. A4).

Millimeters of melt per century (fig. 7e) displays the high variability of melt events, as some centuries do not contain any events. Yet, the running mean (black line) shows distinct spikes, around 4500 to 5000 yrs b2k, 6000 to 6500 yrs b2k and around

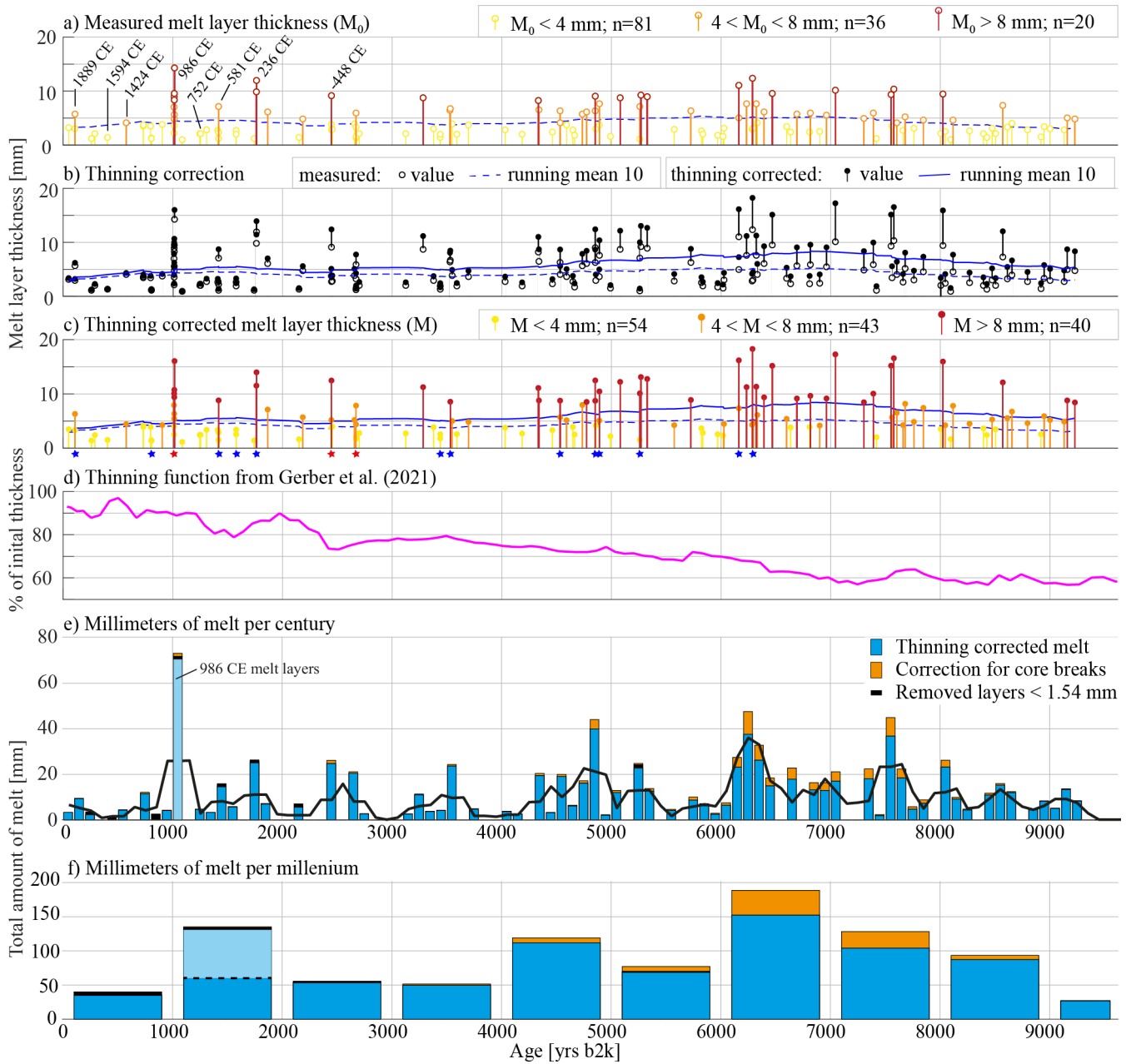


Figure 7. The layer thickness of melt layers is shown by the yellow, orange, and red bars, (smaller 4 mm, between 4 and 8 mm, greater than 8 mm, respectively) and to distinguish events within a short period, the thickness is indicated by circles (measured thickness by open circles, M_0 , and thinning-corrected by closed circles, M). Running mean over 10 events with dashed (measured) and solid blue line (thinning-corrected). Individual correction for thinning (b) using the thinning function from Gerber et al. (2021) shown in d). Labeled in panel a) are events later compared to tree rings with ages in [CE] notation. Stars in c) mark multiple events within five years (blue two events, red three or more). Millimeters of melt per century (e) and millennium (f) (blue bars, calculated from melt layer thicknesses), potentially missed events due to core breaks (orange), removed layers smaller than 1.54 mm (black, see fig. A4), and running mean (black line). Melt layers around the year 986 CE plotted in light blue.

7500 yrs b2k. These coincide with the period of the HCO. The HCO is also pronounced in the amount of melt per millennial (fig. 7f), with a peak in the interval between 6000 and 7000 yrs b2k.

Outstanding in both plots, centuries and millennia, is the peak around 1000 yrs b2k (light blue). The melt event from this period, i.e. 1014 yrs b2k or 986 CE, was of such an intensity, that it leaves an unprecedented spike in the melt record of the past 10,000 years. Here, it is important to note, that this is an event confined to a short period over one or a few summers, and not a signal representative for the entire century or millennium.

4 Discussion

4.1 Integrity of our (and other) melt layer records

If a melt lens is behind bubbles it becomes hard to see in our 2D images, and will probably be classified as uncertain, or missed completely (fig. A2). The prominent and big events will not be missed with our analysis as they are very obvious in line scan images. To further reduce the likeliness of missing events, our analysis was done twice, minimizing operator errors.

We may also miss bubble-free layers in the ice sheet's stratigraphy due to the ice core's restricted diameter. Studies such as Keegan et al. (2014), Schaller (2018), Fegyveresi et al. (2018), Taranczewski et al. (2019), or our coffee experiment (fig. A1) show the high spatial variability of melt lenses in trenches or shallow cores. While the spatial distribution of a melt lens or a layer is not homogeneous over larger areas, our ice core with a diameter of 10 cm is a very narrow sample of the ice column. Keegan et al. (2014) show that big melt events, such as the 1889 CE event are visible in most shallow cores and snowpits and thus prove a widespread distribution. For bigger events, we can therefore assume that our analysis is representative of the largest part of Northern Greenland, while smaller events might be restricted to local areas.

4.2 The highly dynamic EastGRIP site

The EastGRIP ice core is drilled into the NEGIS (fig. 2a), with a surface velocity of 55 m/yr. Gerber et al. (2021) backtrack the location of ice from EastGRIP over time and show that, e.g., 9000 years old ice was deposited 170 (\pm 17) km further southwest and at a 270 m higher elevation. For their calculations Gerber et al. (2021) use today's ice sheet dimensions, but as Vinther et al. (2009) show, the ice sheet elevation has not been constant over the Holocene (fig. 2b). Vinther et al. (2009) suggest that NEGIS' origin, the area somewhere between the NorthGRIP and GRIP sites, was at 150 to 200 m higher elevation at the beginning of the Holocene, compared to today.

Adding the values from Vinther et al. (2009) and Gerber et al. (2021), the true elevation change over the past 9000 years could lie around 400 m. Using the lapse rate estimate of temperatures decreasing by 0.6 to 0.9°C every 100 m of elevation gain (Gardner et al., 2009), we can deduce a temperature change at the EastGRIP drill site of 2.4 to 3.6°C (or 3 ± 0.6 °C) solely by waiting 9000 years, flowing downstream, and without considering any climatic changes. Thus, when analyzing EastGRIP-ice we must take into account the spatial variations with time.

Alley and Anandakrishnan (1995) suggest that an increase in 2°C causes a 7.5-fold increase in melt frequency, by comparing their GISP2 melt layer frequencies to a record from site A (Alley and Koci, 1988). Assuming this linear relationship between melt layers and temperature to be correct, we would expect a more than 10-fold increase in melt frequency for EastGRIP from the Early Holocene to today, solely due to the lowering of the site elevation. An increase of frequency in such magnitude is not supported by our data. On the contrary, the amount of melt and the average thickness of melt layers decreases from the Early Holocene to today (see fig. 7f). Thus, cooling or a decreasing summer insolation, over-weighs the warming of elevation drop. Despite the lower surface elevation today and the corresponding $3\pm0.6^{\circ}\text{C}$ warming, our data suggests that melt events around the HCO have been more intense (fig. 7) and more frequent (fig. A5).

4.3 The EastGRIP melt layer record

In comparison with ice core melt layer records from south western Greenland (Trusel et al., 2018), Renland, coastal Greenland (Taranczewski et al., 2019), or northern Canada (Fisher et al., 2012), the record of 831 mm melt in 10,000 yrs of the EastGRIP ice core is rather low. Here we must keep in mind that the average summer temperature at EastGRIP lays around -25°C , making melt events a rare phenomenon. It is therefore almost surprising that we find 137 melt layers and 424 melt lenses at a site with such cold summers.

4.4 The melt layers of the 986 CE event

When analyzing melt layers on an annual time scale, the well-studied 2012 CE melt event in Greenland (e.g. Nghiem et al., 2012; Bonne et al., 2015; Nilsson et al., 2015) helps our understanding of natural melt events. The infiltration of melt layers from different years into the stratigraphy, could potentially ruin the consistency of, e.g. isotope records assuming the stratigraphy to be linear in time. This certainly adds another factor of complication to the tempo-spatial variability recently observed and discussed (e.g. Steen-Larsen et al., 2011; Münch and Laepple, 2018). In hindsight it is not possible to distinguish between two scenarios: 1) five consecutive years with surface melting each summer, which then create a melt layer in each of the corresponding snow layers, or 2) one large melt and rain event, which creates melt layers scattered across all the snow from the last five years below. For smaller events the first options seems likely. For larger events, creating thick melt layers, the chances are high that melt percolates deep into the wet and warm snowpack, disrupting the stratigraphic order.

In a depth around 138 m, we find nine melt layers and 12 melt lenses over just 50 centimeters (fig. 8). This depth interval represent the years 988 to 982 CE (on GICC05 timescale). Adjusting to the new GICC21 timescale (Sinnl et al., 2021 in review) this corresponds to the years 993 to 987 CE.

According to the thinning function of Gerber et al. (2021), in this depth the layers have been thinned to approximately 90% of their initial thickness (fig. 7d). The thinning function works reliably in firn and ice, yet the melt layers must have been formed while the snow was still loosely packed on the surface. Today, five years on the surface would approximately cover 1.5 meters of the snow pack (Kjær et al., 2021).

The nine melt layers might not represent nine separate events, but could have been created in one single event. It may be possible, that melt water percolated approximately 1.5 m deep into the snowpack and left nine melt layers. All of these layers

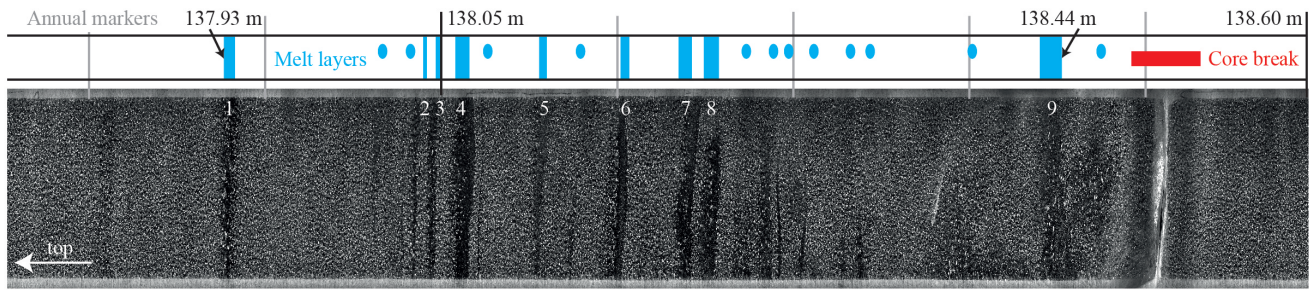


Figure 8. Nine melt layers and 12 melt lenses (blue bars and ellipses, respectively) over of 50 centimeters around 138 m depth. Vertical gray lines represent annual markers. The depth 138.05 m corresponds to the year 986 CE (GICC05) or 991 CE (GICC21).

would thus may have formed within a few days. During the 2012 CE warm event, with rain, at NEEM melt percolated 0.7
 315 m into the snowpack, i.e. half the depth of our event (fig. A1c). This leaves two assumptions: 1) the 986 CE event was more
 intense than the 2012 CE event, or 2) we are looking at multiple summers with surface melt. As shown in fig. 8, layer 1 (137.93
 m) is located one year above layer two, while layer nine is located two years below layer eight. The close proximity of layers
 2 to 8 hints to a single formation event, similar to the 2012 CE event (fig. A1). It could thus be, that three consecutive warm
 summers have created this melt layer sequence.

320 Assuming the melt layers around 986 CE to have formed in one event, then this must have been a long lasting period of high
 temperatures and/or of intense rain fall. Rain events are rare on the Greenland ice sheet and melt events such as the 2012 CE
 event are clearly outstanding with the many melt layer traces they leave. It is also worth noting, that the 1889 CE melt event,
 which is present in most areas and ice cores across Greenland and therefore considered a big event, consists of only two melt
 layers with a total of 8.5 mm melt. The 1889 CE event must therefore not have been as intense as the 986 CE (total of 63.2
 325 mm melt) or the 2012 CE event. The only melt event comparable to the 986 CE event, yet with significantly thinner layers,
 happened around the year 675 BCE (2675 yrs b2k and 328 m depth, fig. 7c) with four melt layers and three melt lenses within
 the stratigraphy of one year, and 11.7 mm of total melt. Thus, events with many melt layers are rare in Greenland, even over
 the course of the entire Holocene.

In a previous version of this work, we noted a possible connection between the 986 CE event and the settlement voyages of
 330 Erik the Red from Iceland to Greenland in the same year. Applying the GICC21 timescale (Sinnl et al., 2021) and considering
 the melt layers (fig. 8) to be three events, then these would be the years 993, 991, and 988 CE. This would date to a few years
 after the Vikings have reached Greenland and could have provided the Nordic settlers with warm summers in their first years
 on Greenland. Nevertheless, the 986 CE melt layer marks the beginning of consecutive warm periods which are also preserved
 in tree ring data (see next section).

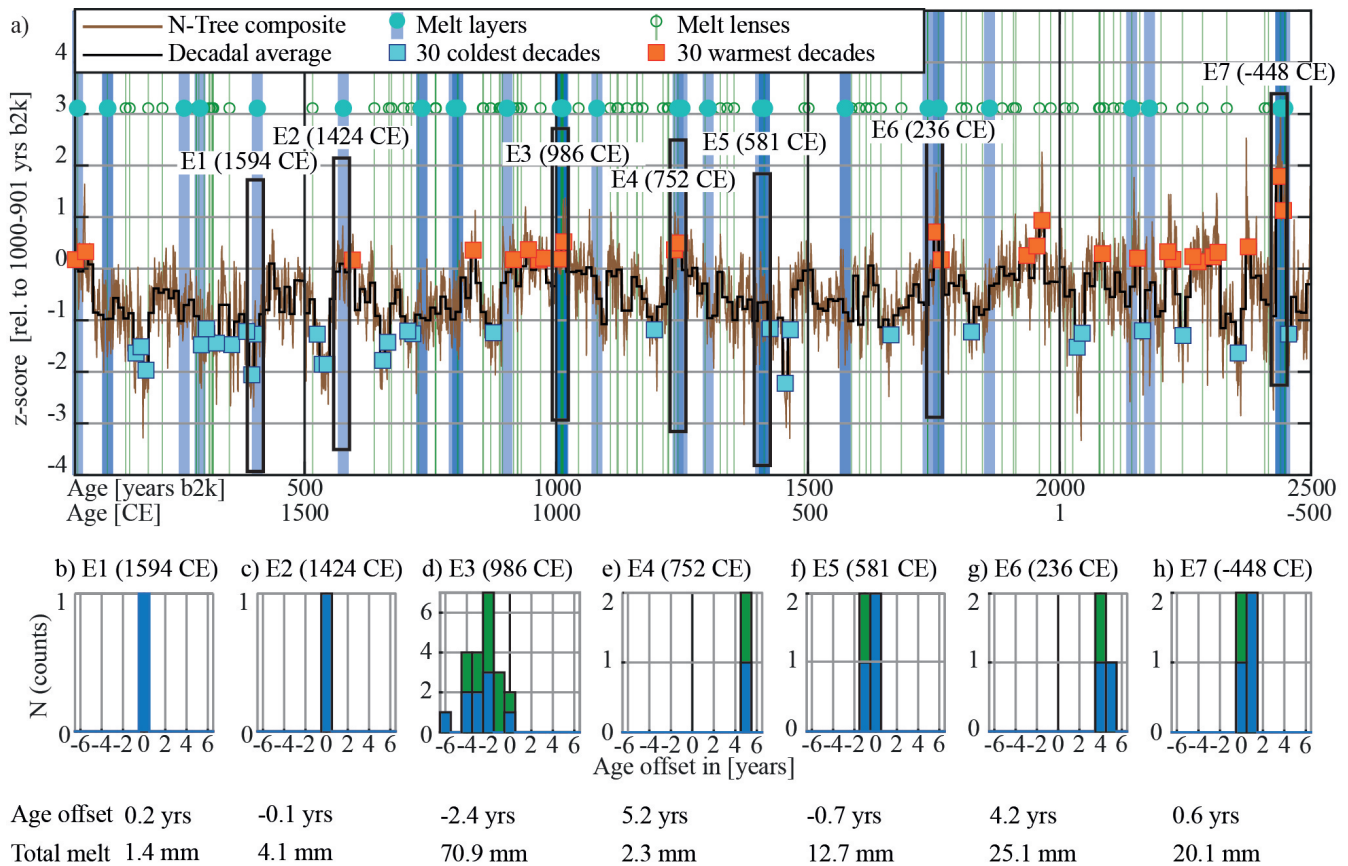


Figure 9. Tree-ring growth anomaly (Sigl et al., 2015) compared to the EastGRIP melt record from 44 to 2500 yrs b2k. a) The tree-ring growth anomaly (brown) was averaged to decadal resolution (black) and the 30 warmest and 30 coldest decades were marked as orange and light blue boxes, respectively. Vertical bars highlight melt layers (blue) and lenses (green) at the corresponding age. Seven melt events (E1 to E7) are highlighted by black boxes. b-h) Histograms of the age offset of the melt events from the largest tree-ring growth year, within ± 6 years (layers in blue, lenses in green). The exceptional 986 CE event (E3) is younger than the tree ring maximum by about 2.4 years. Entire figure is on NS1-2011 tree ring timescale, only exception are dates of events, e.g. 986 CE, which are on GICC05 for consistency.

335 4.5 Melt layers and Northern Hemisphere tree rings

We use the tree ring data (Sigl et al., 2015) to compare to melt layers. We evaluated the age offset of seven melt events (see fig. 7a) to the highest peak in the tree ring record (fig. 9a), within a ± 6 -year window around the melt event (fig. 9b to h). Melt events lay very close to a tree ring peak, in most cases within the same year. Two events show an offset of four to five years to the highest peak within the ± 6 -year window (E4 and E6, fig. 9e,g, respectively). We find a slightly smaller peak around the same year as the melt layers. Thus, we attribute this offset to incorrect peak assignment. All highlighted events (black boxes,

E1 to E7) have at least one tree ring peak (warm anomaly) in very close proximity. For the 986 CE event (E3, fig. 9d), the most outstanding melt event in our record, we find a tree ring warm-year which is about 2.4 years older.

A more recent, 2000 year, temperature reconstruction from Büntgen et al. (2020) shows a distinct tree ring peak in the year 990 CE, which coincides with our E3 event, which spans across the year 990 CE on the the GICC21 timescale (Sinnl et al., 2021). The shift of some of the other tree ring peaks by a few years from the compilation of Sigl et al. (2015) to Büntgen et al. (2020) still leaves our melt layers in close proximity of these peaks.

Melting at EastGRIP might not be synchronous with all tree ring peaks, but still offers some insight to the correlation of melt and tree ring growth on a larger geographic scale. This is also the case for volcanic eruptions: many volcanic events do not correspond to deep cooling in the tree ring records, although local minima are often observed in correspondence. Due to the age uncertainty of melt events and difficulties in time-scale translations, we cannot evaluate a more precise age-offset. Moreover, even though more melting occurs during tree ring warm-decades, not every prominent peak in the tree ring record has melt events in its proximity.

The location of EastGRIP might not represent the complexity of the climatic dynamics that produces tree ring growth anomalies at scattered locations around the Northern Hemisphere, but the occurrence of more melt in warm periods and in proximity of some of the warmest years suggests a partial correlation. We expect that future studies could improve the results we have presented, in particular for the correlation of the melt events at EastGRIP with other ice cores and with more temperature records from the northern Hemisphere.

5 Conclusion

We have created a melt record from the EastGRIP ice core covering the largest part of the Holocene. This record is only the second one, after Alley and Anandakrishnan (1995), that covers central Greenland. In the Early and beginning of the Middle Holocene, we find the thickest melt layers (fig. 7c) and also more melt per century or millennia than in the younger part of the Holocene (fig. 7e,f). Nevertheless, the most occurrences of melt layers within a few years lay in the Late Holocene (fig. 7c), e.g. the 2012 CE, the 986 CE, or 675 BCE events.

The melt event leaving the most melt layers in our record is the 986 CE event, followed by the 675 BCE event. The 2012 CE event is not displayed in our record but seems to leave similar traces as the 986 CE event (fig. A1). So far, the 986 CE and 2012 CE melt events are unprecedented in the Holocene. This extends the statement of Trusel et al. (2018), who find the 2012 CE event to be unprecedented in the most recent 350 years. Although the 2012 CE melt, and rain, event is considered an exception it could be a hint to what we can expect for future summers in Greenland as global warming proceeds.

In our melt event record, we distinguish between melt layers and lenses and compare the most recent 2500 years to the tree ring temperature anomaly record from Sigl et al. (2015). Hereby we find that some peaks in the melt events and tree ring data align (with an offset of a few years, see above). The large melt events stand out in the tree ring record from Sigl et al. (2015, fig. 9) and also in the record of Büntgen et al. (2020, not compared in detail here). Warm events found in ice cores and tree rings therefore hint at outstanding warm summers being a phenomenon over the entire Northern Hemisphere. While this is not

strictly in agreement with our understanding of atmospheric circulations (e.g. Bonne et al., 2015; Hanna et al., 2016; Graeter et al., 2018), the effect could also be restricted to some trees used in the tree ring composite, introducing a warm bias for these certain years.

The value of a melt record from the EastGRIP ice stream ice core is its change of location and elevation over the past 9000 years. Today, the highly dynamic EastGRIP site is 170 km further north-northeast and 400 m lower than 9000 years ago. With a corresponding lapse rate, of 0.6 to 0.9°C per 100 m, the temperature has increased by $3 \pm 0.6^\circ\text{C}$ over the past 9000 years. This temperature change is solely connected to the drop of elevation and not any climatic changes. Yet, this change holds implications for climate, as we find more and thicker melt layers in the Early Holocene than today (fig. 7), while an increase in temperature over $3 \pm 0.6^\circ\text{C}$ would suggest more and thicker melt layers today. This infers that the local warming caused by elevation drop does not compensate the summer temperature cooling over the Holocene. Our data therefore strongly suggest that Greenland summer temperatures must have been more than $3 \pm 0.6^\circ\text{C}$ warmer during the Early Holocene than today. The full-year average temperature from the GRIP borehole temperature follows the same trend as our melt layer proxy for summer temperatures, suggesting a stable Middle Holocene temperature and a decrease, with fluctuations, over the Early Holocene.

Melt records from central Greenland deep ice cores, e.g. GISP2 or EastGRIP, are subjected to less horizontal thinning in the Early Holocene than shallower ice cores, e.g. the RECAP ice core (Alley and Anandakrishnan, 1995; Taranczewski et al., 2019). This holds the advantage, that the Early Holocene melt record is preserved in a higher resolution and our melt layer record thus differs from the melt reconstruction from Taranczewski et al. (2019). Nevertheless, due to the bubble-clathrate transition at around 1100 m depth, our melt layer records ends approximately 9300 years before today, as does the record of Alley and Anandakrishnan (1995). Establishing melt layer records below this depth/age remains a challenge due to the lack of bubbles and therefore the inability to find bubble-free layers. An attempt to approach this problem would be to analyze the bubble distribution in line scan images and the first steps have been done by Morcillo et al. (2020).

Our melt layer record can lay the basis to better understand summer temperatures in the Holocene, as the melt layers pinpoint warm events. The frequency or temporal distribution of these events can be incorporated in climate reconstructions or modeling studies (e.g. McCrystall et al., 2021). Melt layer records are therefore valuable climate archives, preserving single warm events over the course of millennia.

Author contribution

400 Initial idea of manuscript and data acquisition by JW. Tree ring to melt comparison, statistics, and verification of time scale by GS, idea of tree ring comparison by AS. Support on melt layers in ice cores in general came from AS, JF, SK, and DDJ. Coffee experiment and melt layer definition by SK and JW. NEEM snowpit data and input by HAK and PV. Climatic interpretations and ice sheet evolution by BMV, AS, and JW. Physical properties of melt layers and their appearance by IW and SK. JW prepared the manuscript with contributions and revisions from all co-authors.

405 Competing interests

The authors declare that they have no conflict of interest.

Acknowledgements

EastGRIP is directed and organized by the Centre for Ice and Climate at the Niels Bohr Institute, University of Copenhagen. It is supported by funding agencies and institutions in Denmark (A. P. Møller Foundation, University of Copenhagen), USA
410 (US National Science Foundation, Office of Polar Programs), Germany (Alfred Wegener Institute, Helmholtz Centre for Polar and Marine Research), Japan (National Institute of Polar Research and Arctic Challenge for Sustainability), Norway (University of Bergen and Bergen Research Foundation), Switzerland (Swiss National Science Foundation), France (French Polar Institute Paul-Emile Victor, Institute for Geosciences and Environmental research) and China (Chinese Academy of Sciences and Beijing Normal University). JW, AS, BMV, SK, and DDJ thank the Villum Foundation, as this work was supported by
415 the Villum Investigator Project IceFlow (NR. 16572). GS acknowledges support via the ChronoClimate project funded by the Carlsberg Foundation. IW acknowledges HGF funding (VH-NG-802). The authors thank the reviewers, two anonymous and Elizabeth Thomas, for their comments and greatly improving the manuscript throughout the process. The authors also thank editor Denis-Didier Rousseau for handling the process.

Data availability

420 Primary data are available on Pangaea (Weikusat et al., 2020, <https://doi.org/10.1594/PANGAEA.925014>). The record of melt layer and other bubble-free features is available on ERDA (<https://erda.ku.dk/archives/cb0dbb0d7a3f7b83cfb0890562ebcc20/published-archive.html>) and will also be uploaded to Pangaea.

References

- 425 Alley, R. and Koci, B.: Ice-Core Analysis at Site A, Greenland: Preliminary Results, *Annals of Glaciology*, 10, 1–4, <https://doi.org/10.3189/s0260305500004067>, 1988.
- Alley, R. B. and Anandakrishnan, S.: Variations in melt-layer frequency in the GISP2 ice core: implications for Holocene summer temperatures in central Greenland, *Annals of Glaciology*, 21, 64–70, <https://doi.org/10.3189/s0260305500015615>, 1995.
- Alley, R. B., Gow, A. J., Meese, D. A., Fitzpatrick, J. J., and Waddington, E. D.: Grain-scale processes, folding, and stratigraphic, *Journal of Geophysical Research*, 102, 26 819–26 830, 1997.
- 430 Axford, Y., de Vernal, A., and Osterberg, E. C.: Past Warmth and Its Impacts During the Holocene Thermal Maximum in Greenland, *Annual Review of Earth and Planetary Sciences*, 49, 279–307, <https://doi.org/10.1146/annurev-earth-081420-063858>, 2021.
- Badgeley, J. A., Steig, E. J., Hakim, G. J., and Fudge, T. J.: Greenland temperature and precipitation over the last 20000 years using data assimilation, *Climate of the Past*, 16, 1325–1346, <https://doi.org/10.5194/cp-16-1325-2020>, 2020.
- 435 Bennartz, R., Shupe, M. D., Turner, D. D., Walden, V. P., Steffen, K., Cox, C. J., Kulie, M. S., Miller, N. B., and Pettersen, C.: July 2012 Greenland melt extent enhanced by low-level liquid clouds, *Nature*, 496, 83–86, <https://doi.org/10.1038/nature12002>, 2013.
- Berger, A. and Loutre, M. F.: Insolation values for the climate of the last 10 million years, *Quaternary Science Reviews*, 10, 297–317, [https://doi.org/10.1016/0277-3791\(91\)90033-Q](https://doi.org/10.1016/0277-3791(91)90033-Q), 1991.
- Büntgen, U., Arseneault, D., Étienne Boucher, Churakova (Sidorova), O. V., Gennaretti, F., Crivellaro, A., Hughes, M. K., Kirdyanov, A. V., Klippel, L., Krusic, P. J., Linderholm, H. W., Ljungqvist, F. C., Ludescher, J., McCormick, M., Myglan, V. S., Nicolussi, K., Piermattei, A., Oppenheimer, C., Reinig, F., Sigl, M., Vaganov, E. A., and Esper, J.: Prominent role of volcanism in Common Era climate variability and human history, *Dendrochronologia*, 64, 125 757, <https://doi.org/https://doi.org/10.1016/j.dendro.2020.125757>, 2020.
- 440 Bonne, J. L., Steen-Larsen, H. C., Risi, C., Werner, M., Sodemann, H., Lacour, J. L., Fettweis, X., Cesana, G., Delmotte, M., Cattani, O., Vallelonga, P., Kjær, H. A., Clerbaux, C., Sveinbjörnsdóttir, Á. E., and Masson-Delmotte, V.: The summer 2012 Greenland heat wave: In situ and remote sensing observations of water vapor isotopic composition during an atmospheric river event, *Journal of Geophysical Research*, 120, 2970–2989, <https://doi.org/10.1002/2014JD022602>, 2015.
- 445 Bova, S., Rosenthal, Y., Liu, Z., Godad, S. P., and Yan, M.: Seasonal origin of the thermal maxima at the Holocene and the last interglacial, *Nature*, 589, 548–553, <https://doi.org/10.1038/s41586-020-03155-x>, 2021.
- Brunt, D.: The adiabatic lapse-rate for dry and saturated air, *Quarterly Journal of the Royal Meteorological Society*, 59, 351–360, <https://doi.org/https://doi.org/10.1002/qj.49705925204>, 1933.
- 450 Buizert, C., Martinerie, P., Petrenko, V. V., Severinghaus, J. P., Trudinger, C. M., Witrant, E., Rosen, J. L., Orsi, A. J., Rubino, M., Etheridge, D. M., Steele, L. P., Hogan, C., Laube, J. C., Sturges, W. T., Levchenko, V. A., Smith, A. M., Levin, I., Conway, T. J., Dlugokencky, E. J., Lang, P. M., Kawamura, K., Jenk, T. M., White, J. W., Sowers, T., Schwander, J., and Blunier, T.: Gas transport in firn: Multiple-tracer characterisation and model intercomparison for NEEM, Northern Greenland, *Atmospheric Chemistry and Physics*, 12, 4259–4277, <https://doi.org/10.5194/acp-12-4259-2012>, 2012.
- Buizert, C., Keisling, B. A., Box, J. E., He, F., Carlson, A. E., Sinclair, G., and DeConto, R. M.: Greenland-Wide Seasonal Temperatures During the Last Deglaciation, *Geophysical Research Letters*, 45, 1905–1914, <https://doi.org/10.1002/2017GL075601>, 2018.
- Cohen, K. M., Finney, S. C., Gibbard, P. L., and Fan, J. X.: International Chronostratigraphic Chart, The ICS International Chronostratigraphic Chart, 36, 199–204, <http://www.stratigraphy.org/ICSchart/ChronostratChart2016-04.pdf>, 2016.

- 460 Community Members, N.: Eemian interglacial reconstructed from a Greenland folded ice core, *Nature*, 493, 489–494, <https://doi.org/10.1038/nature11789>, 2013.
- Dahl-Jensen, D., Mosegaard, K., Gundestrup, N., Clow, G. D., Johnsen, S. J., Hansen, A. W., and Balling, N.: Past temperatures directly from the Greenland Ice Sheet, *Science*, 282, 268–271, <https://doi.org/10.1126/science.282.5387.268>, 1998.
- Dalton, A. S., Margold, M., Stokes, C. R., Tarasov, L., Dyke, A. S., Adams, R. S., Allard, S., Arends, H. E., Atkinson, N., Attig, J. W.,
 465 Barnett, P. J., Barnett, R. L., Batterson, M., Bernatchez, P., Borns, H. W., Breckenridge, A., Briner, J. P., Brouard, E., Campbell, J. E., Carlson, A. E., Clague, J. J., Curry, B. B., Daigneault, R. A., Dubé-Loubert, H., Easterbrook, D. J., Franz, D. A., Friedrich, H. G., Funder, S., Gauthier, M. S., Gowan, A. S., Harris, K. L., Hétu, B., Hooyer, T. S., Jennings, C. E., Johnson, M. D., Kehew, A. E., Kelley, S. E., Kerr, D., King, E. L., Kjeldsen, K. K., Knaeble, A. R., Lajeunesse, P., Lakeman, T. R., Lamothe, M., Larson, P., Lavoie, M., Loope, H. M., Lowell, T. V., Lusardi, B. A., Manz, L., McMartin, I., Nixon, F. C., Occhietti, S., Parkhill, M. A., Piper, D. J., Pronk, A. G., Richard, P. J.,
 470 Ridge, J. C., Ross, M., Roy, M., Seaman, A., Shaw, J., Stea, R. R., Teller, J. T., Thompson, W. B., Thorleifson, L. H., Utting, D. J., Veillette, J. J., Ward, B. C., Weddle, T. K., and Wright, H. E.: An updated radiocarbon-based ice margin chronology for the last deglaciation of the North American Ice Sheet Complex, *Quaternary Science Reviews*, 234, <https://doi.org/10.1016/j.quascirev.2020.106223>, 2020.
- Das, S. B. and Alley, R. B.: Characterization and formation of melt layers in polar snow : observations and experiments from West Antarctica, *Journal of Glaciology*, 51, 307–312, 2005.
- 475 Dash, J. G., Rempel, A. W., and Wettlaufer, J. S.: The physics of premelted ice and its geophysical consequences, *Reviews of Modern Physics*, 78, 695–741, <https://doi.org/10.1103/RevModPhys.78.695>, 2006.
- Faria, S. H., Kipfstuhl, S., and Lambrecht, A.: The EPICA-DML Deep Ice Core, Springer-Verlag GmbH Germany, Berlin, 2018.
- Fegyveresi, J. M., Alley, R. B., Muto, A., Orsi, A. J., and Spencer, M. K.: Surface formation, preservation, and history of low-porosity crusts at the WAIS Divide site, West Antarctica, *Cryosphere*, 12, 325–341, <https://doi.org/10.5194/tc-12-325-2018>, 2018.
- 480 Fisher, D., Zheng, J., Burgess, D., Zdanowicz, C., Kinnard, C., Sharp, M., and Bourgeois, J.: Recent melt rates of Canadian arctic ice caps are the highest in four millennia, *Global and Planetary Change*, 84–85, 3–7, <https://doi.org/10.1016/j.gloplacha.2011.06.005>, 2012.
- Fisher, D. A., Koerner, R. M., and Reeh, N.: Holocene climatic records from Agassiz Ice Cap, Ellesmere Island, NWT, Canada, *Holocene*, 5, 19–24, <https://doi.org/10.1177/095968369500500103>, 1995.
- Fritzsche, D., Schütt, R., Meyer, H., Miller, H., Wilhelms, F., Opel, T., and Savatyugin, L. M.: A 275 year ice-core record from Akademii
 485 Nauk ice cap, Severnaya Zemlya, Russian Arctic, *Annals of Glaciology*, 42, 361–366, <https://doi.org/10.3189/172756405781812862>, 2005.
- Gardner, A. S., Sharp, M. J., Koerner, R. M., Labine, C., Boon, S., Marshall, S. J., Burgess, D. O., and Lewis, D.: Near-surface temperature lapse rates over arctic glaciers and their implications for temperature downscaling, *Journal of Climate*, 22, 4281–4298, <https://doi.org/10.1175/2009JCLI2845.1>, 2009.
- 490 Gerber, T. A., Hvidberg, C. S., Rasmussen, S. O., Franke, S., Sinnl, G., Grinsted, A., Jansen, D., and Dahl-jensen, D.: Upstream flow effects revealed in the EastGRIP ice core using a Monte Carlo inversion of a two-dimensional ice-flow model, *The Cryosphere*, 2021.
- Graeter, K. A., Osterberg, E. C., Ferris, D. G., Hawley, R. L., Marshall, H. P., Lewis, G., Meehan, T., McCarthy, F., Overly, T., and Birkel, S. D.: Ice Core Records of West Greenland Melt and Climate Forcing, *Geophysical Research Letters*, 45, 3164–3172, <https://doi.org/10.1002/2017GL076641>, 2018.
- 495 Hanna, E., Cropper, T. E., Hall, R. J., and Cappelen, J.: Greenland Blocking Index 1851–2015: a regional climate change signal, *International Journal of Climatology*, 36, 4847–4861, <https://doi.org/10.1002/joc.4673>, 2016.

- Herron, M. M., Herron, S. L., and Langway, C. C.: Climatic signal of ice melt features in southern Greenland, *Nature*, 293, 389–391, <https://doi.org/10.1038/293389a0>, 1981.
- Humphrey, N. F., Harper, J. T., and Pfeffer, W. T.: Thermal tracking of meltwater retention in Greenland ’ s accumulation area, *Journal of Geophysical Research*, 117, 1–11, <https://doi.org/10.1029/2011JF002083>, 2012.
- Hvidberg, C. S., Grinsted, A., Dahl-Jensen, D., Khan, S. A., Kusk, A., Andersen, J. K., Neckel, N., Solgaard, A., Karlsson, N. B., Kjar, H. A., and Vallelonga, P.: Surface velocity of the Northeast Greenland Ice Stream (NEGIS): Assessment of interior velocities derived from satellite data by GPS, *Cryosphere*, 14, 3487–3502, <https://doi.org/10.5194/tc-14-3487-2020>, 2020.
- Jansen, D., Llorens, M. G., Westhoff, J., Steinbach, F., Kipfstuhl, S., Bons, P. D., Griera, A., and Weikusat, I.: Small-scale disturbances in the stratigraphy of the NEEM ice core: Observations and numerical model simulations, *The Cryosphere*, 10, 359–370, <https://doi.org/10.5194/tc-10-359-2016>, 2016.
- Kameda, T., Narita, H., Shoji, H., Nishio, F., Fujii, Y., and Watanabe, O.: Melt features in ice cores from site J, souther Greenland: some implications for summer cliamte since AD 1550, *Annals of Glaciology*, pp. 51–58, 1995.
- Keegan, K. M., Albert, M. R., McConnell, J. R., and Baker, I.: Climate change and forest fires synergistically drive widespread melt events of the Greenland Ice Sheet, *Proceedings of the National Academy of Sciences of the United States of America*, 111, 7964–7967, <https://doi.org/10.1073/pnas.1405397111>, 2014.
- Kipfstuhl, S., Pauer, F., Kuhs, W. F., and Shoji, H.: Air bubbles and clathrate hydrates in the transition zone of the NGRIP deep ice core, *Geophysical Research Letters*, 28, 591–594, <https://doi.org/10.1029/1999GL006094>, 2001.
- Kjær, H. A., Lolk Hauge, L., Simonsen, M., Yoldi, Z., Koldtoft, I., Hörhold, M., Freitag, J., Kipfstuhl, S., Svensson, A., and Vallelonga, P.: A portable lightweight in situ analysis (LISA) box for ice and snow analysis, *The Cryosphere*, 15, 3719–3730, <https://doi.org/10.5194/tc-15-3719-2021>, 2021.
- Koerner, R. M. and Fisher, D. A.: A record of Holocene summer climate from a Canadian high-Arctic ice core, *Nature*, 343, 630–631, <https://doi.org/10.1038/343630a0>, 1990.
- Lecavalier, B. S., Milne, G. A., Vinther, B. M., Fisher, D. A., Dyke, A. S., and Simpson, M. J.: Revised estimates of Greenland ice sheet thinning histories based on ice-core records, *Quaternary Science Reviews*, 63, 73–82, <https://doi.org/10.1016/j.quascirev.2012.11.030>, 2013.
- Lecavalier, B. S., Fisher, D. A., Milne, G. A., Vinther, B. M., Tarasov, L., Huybrechts, P., Lacelle, D., Main, B., Zheng, J., Bourgeois, J., and Dyke, A. S.: High Arctic Holocene temperature record from the Agassiz ice cap and Greenland ice sheet evolution, *Proceedings of the National Academy of Sciences of the United States of America*, 114, 5952–5957, <https://doi.org/10.1073/pnas.1616287114>, 2017.
- Llorens, M. G., Griera, A., Steinbach, F., Bons, P. D., Gomez-Rivas, E., Jansen, D., Roessiger, J., Lebensohn, R. A., and Weikusat, I.: Dynamic recrystallization during deformation of polycrystalline ice: Insights from numerical simulations, *Philosophical Transactions of the Royal Society A: Mathematical, Physical and Engineering Sciences*, 375, <https://doi.org/10.1098/rsta.2015.0346>, 2017.
- McCrystall, M. R., Stroeve, J., Serreze, M., Forbes, B. C., and Screen, J. A.: New climate models reveal faster and larger increases in Arctic precipitation than previously projected, *Nature communications*, 12, 1–12, 2021.
- McGwire, K. C., Hargreaves, G. M., Alley, R. B., Popp, T. J., Reusch, D. B., Spencer, M. K., and Taylor, K. C.: An integrated system for optical imaging of ice cores, *Cold Regions Science and Technology*, 53, 216–228, <https://doi.org/10.1016/j.coldregions.2007.08.007>, 2008.
- Mojtabavi, S., Wilhelms, F., Cook, E., Davies, S., Sinnl, G., Skov Jensen, M., Dahl-Jensen, D., Svensson, A., Vinther, B., Kipfstuhl, S., Jones, G., Karlsson, N., Faria, S. H., Gkinis, V., Kjær, H., Erhardt, T., Berben, S., Nisancioglu, K., Koldtoft, I., and Rasmussen, S. O.:

- 535 A first chronology for the East GRenland Ice-core Project (EGRIP) over the Holocene and last glacial termination, *Climate of the Past Discussions*, 16, 2359—2380, <https://doi.org/10.5194/cp-16-2359-2020>, 2020.
- Monnin, E., Steig, E. J., Siegenthaler, U., Kawamura, K., Schwander, J., Stauffer, B., Stocker, T. F., Morse, D. L., Barnola, J. M., Bellier, B., Raynaud, D., and Fischer, H.: Evidence for substantial accumulation rate variability in Antarctica during the Holocene, through synchronization of CO₂ in the Taylor Dome, Dome C and DML ice cores, *Earth and Planetary Science Letters*, 224, 45–54, <https://doi.org/10.1016/j.epsl.2004.05.007>, 2004.
- 540 Morcillo, G., Faria, S. H., and Kipfstuhl, S.: Unravelling Antarctica’s past through the stratigraphy of a deep ice core: an image-analysis study of the EPICA-DML line-scan images, *Quaternary International*, <https://doi.org/10.1016/j.quaint.2020.07.011>, 2020.
- Mote, T. L.: Greenland surface melt trends 1973-2007: Evidence of a large increase in 2007, *Geophysical Research Letters*, 34, 1–5, <https://doi.org/10.1029/2007GL031976>, 2007.
- 545 Münch, T. and Laepple, T.: What climate signal is contained in decadal - To centennial-scale isotope variations from Antarctic ice cores?, *Climate of the Past*, 14, 2053–2070, <https://doi.org/10.5194/cp-14-2053-2018>, 2018.
- Neff, P. D.: A review of the brittle ice zone in polar ice cores, *Annals of Glaciology*, 55, 72–82, <https://doi.org/10.3189/2014AoG68A023>, 2014.
- Nghiem, S. V., Hall, D. K., Mote, T. L., Tedesco, M., Albert, M. R., Keegan, K., Shuman, C. A., DiGirolamo, N. E., and Neumann, G.: The extreme melt across the Greenland ice sheet in 2012, *Geophysical Research Letters*, 39, 6–11, <https://doi.org/10.1029/2012GL053611>, 2012.
- 550 Nilsson, J., Vallelonga, P., Simonsen, S. B., Sørensen, L. S., Forsberg, R., Dahl-Jensen, D., Hirabayashi, M., Goto-Azuma, K., Hvidberg, C. S., Kjær, H. A., and Satow, K.: Greenland 2012 melt event effects on CryoSat-2 radar altimetry, *Geophysical Research Letters*, 42, 3919–3926, <https://doi.org/10.1002/2015GL063296>, 2015.
- 555 NorthGRIPmembers: High-resolution record of Northern Hemisphere climate extending into the last interglacial period, *Nature*, 431, 147–151, 2004.
- Orsi, A. J., Kawamura, K., Fegyveresi, J. M., Headly, M. A., Alley, R. B., and Severinghaus, J. P.: Differentiating bubble-free layers from Melt layers in ice cores using noble gases, *Journal of Glaciology*, 61, 585–594, <https://doi.org/10.3189/2015JoG14J237>, 2015.
- Pfeffer, W. T. and Humphrey, N. F.: Fortmation of ice layers by infiltration and refreezing of meltwater, *Annals of Glaciology*, 26, 83–91, 1998.
- 560 Rasmussen, S. O., Andersen, K. K., Svensson, A. M., Steffensen, J. P., Vinther, B. M., Clausen, H. B., Siggaard-Andersen, M. L., Johnsen, S. J., Larsen, L. B., Dahl-Jensen, D., Bigler, M., Röthlisberger, R., Fischer, H., Goto-Azuma, K., Hansson, M. E., and Ruth, U.: A new Greenland ice core chronology for the last glacial termination, *Journal of Geophysical Research Atmospheres*, 111, 1–16, <https://doi.org/10.1029/2005JD006079>, 2006.
- 565 Rasmussen, S. O., Vinther, B. M., Clausen, H. B., and Andersen, K. K.: Early Holocene climate oscillations recorded in three Greenland ice cores, *Quaternary Science Reviews*, 26, 1907–1914, <https://doi.org/10.1016/j.quascirev.2007.06.015>, 2007.
- Schaller, C. F.: Towards understanding the signal formation in polar snow, firn and ice using X-ray computed tomography, PhD Thesis, p. 68, <https://doi.org/10.1088/1751-8113/44/8/085201>, 2018.
- Schaller, C. F., Freitag, J., Kipfstuhl, S., Laepple, T., Christian Steen-Larsen, H., and Eisen, O.: A representative density profile of the North Greenland snowpack, *Cryosphere*, 10, 1991–2002, <https://doi.org/10.5194/tc-10-1991-2016>, 2016.
- 570 Shoji, H. and Langway, C.: HYDRATE-BUBBLE . TRANSFORMATION PROCESS IN GLACIER ICE, *Journal de Physique*, 3, 551–556, 1987.

- Sigl, M., Winstrup, M., McConnell, J. R., Welten, K. C., Plunkett, G., Ludlow, F., Büntgen, U., Caffee, M., Chellman, N., Dahl-Jensen, D., Fischer, H., Kipfstuhl, S., Kostick, C., Maselli, O. J., Mekhaldi, F., Mulvaney, R., Muscheler, R., Pasteris, D. R., Pilcher, J. R., Salzer, M., Schüpbach, S., Steffensen, J. P., Vinther, B. M., and Woodruff, T. E.: Timing and climate forcing of volcanic eruptions for the past 2,500 years, *Nature*, 523, 543–549, <https://doi.org/10.1038/nature14565>, 2015.
- Simonsen, M. F., Baccolo, G., Blunier, T., Borunda, A., Delmonte, B., Frei, R., Goldstein, S., Grinsted, A., Kjær, H. A., Sowers, T., Svensson, A., Vinther, B., Vladimirova, D., Winckler, G., Winstrup, M., and Vallenga, P.: East Greenland ice core dust record reveals timing of Greenland ice sheet advance and retreat, *Nature Communications*, 10, <https://doi.org/10.1038/s41467-019-12546-2>, 2019.
- Sinnl, G., Winstrup, M., Erhardt, T., Cook, E., Jensen, C., Svensson, A., Vinther, B. M., Muscheler, R., and Rasmussen, S. O.: A multi-ice-core, annual-layer-counted Greenland ice-core chronology for the last 3800 years: GICC21, *Climate of the Past Discussions*, 2021, 1–34, <https://doi.org/10.5194/cp-2021-155>, 2021.
- Steen-Larsen, H. C., Masson-Delmotte, V., Sjolte, J., Johnsen, S. J., Vinther, B. M., Bréon, F. M., Clausen, H. B., Dahl-Jensen, D., Falourd, S., Fettweis, X., Gallée, H., Jouzel, J., Kageyama, M., Lerche, H., Minster, B., Picard, G., Punge, H. J., Risi, C., Salas, D., Schwander, J., Steffen, K., Sveinbjörnsdóttir, A. E., Svensson, A., and White, J.: Understanding the climatic signal in the water stable isotope records from the NEEM shallow firn/ice cores in northwest Greenland, *Journal of Geophysical Research Atmospheres*, 116, 1–20, <https://doi.org/10.1029/2010JD014311>, 2011.
- Steinbach, F., Bons, P. D., Giera, A., Jansen, D., Llorens, M. G., Roessiger, J., and Weikusat, I.: Strain localization and dynamic recrystallization in the ice-air aggregate: A numerical study, *Cryosphere*, 10, 3071–3089, <https://doi.org/10.5194/tc-10-3071-2016>, 2016.
- Svensson, A., Nielsen, S. W., Kipfstuhl, S., Johnsen, S. J., Steffensen, J. P., Bigler, M., Ruth, U., and Röthlisberger, R.: Visual stratigraphy of the North Greenland Ice Core Project (NorthGRIP) ice core during the last glacial period, *Journal of Geophysical Research: Atmospheres*, 110, 1–11, <https://doi.org/10.1029/2004JD005134>, 2005.
- Taranczewski, T., Freitag, J., Eisen, O., Vinther, B., Wahl, S., and Kipfstuhl, S.: 10,000 years of melt history of the 2015 Renland ice core, EastGreenland, *The Cryosphere Discussions*, pp. 1–16, <https://doi.org/10.5194/tc-2018-280>, 2019.
- Tedesco, M., Fettweis, X., Mote, T., Wahr, J., Alexander, P., Box, J. E., and Wouters, B.: Evidence and analysis of 2012 Greenland records from spaceborne observations, a regional climate model and reanalysis data, *The Cryosphere*, 7, 615–630, <https://doi.org/10.5194/tc-7-615-2013>, 2013.
- Thomas, E. R., Wolff, E. W., Mulvaney, R., Steffensen, J. P., Johnsen, S. J., Arrowsmith, C., White, J. W., Vaughn, B., and Popp, T.: The 8.2 ka event from Greenland ice cores, *Quaternary Science Reviews*, 26, 70–81, <https://doi.org/10.1016/j.quascirev.2006.07.017>, 2007.
- Trusel, L. D., Das, S. B., Osman, M. B., Evans, M. J., Smith, B. E., Fettweis, X., McConnell, J. R., Noël, B. P., and van den Broeke, M. R.: Nonlinear rise in Greenland runoff in response to post-industrial Arctic warming, *Nature*, 564, 104–108, <https://doi.org/10.1038/s41586-018-0752-4>, 2018.
- Uchida, T., Yasuda, K., Oto, Y., Shen, R., and Ohmura, R.: Natural supersaturation conditions needed for nucleation of air-clathrate hydrates in deep ice sheets, *Journal of Glaciology*, 60, 1135–1139, <https://doi.org/10.3189/2014JoG13J232>, 2014.
- Vallenga, P., Christianson, K., Alley, R. B., Anandakrishnan, S., Christian, J. E., Dahl-Jensen, D., Gkinis, V., Holme, C., Jacobel, R. W., Karlsson, N. B., Keisling, B. A., Kipfstuhl, S., Kjær, H. A., Kristensen, M. E., Muto, A., Peters, L. E., Popp, T., Riverman, K. L., Svensson, A. M., Tibuleac, C., Vinther, B. M., Weng, Y., and Winstrup, M.: Initial results from geophysical surveys and shallow coring of the Northeast Greenland Ice Stream (NEGIS), *Cryosphere*, 8, 1275–1287, <https://doi.org/10.5194/tc-8-1275-2014>, 2014.

- Vinther, B. M., Clausen, H. B., Johnsen, S. J., Rasmussen, S. O., Andersen, K. K., Buchardt, S. L., Dahl-Jensen, D., Seierstad, I. K.,
610 Siggaard-Andersen, M. L., Steffensen, J. P., Svensson, A., Olsen, J., and Heinemeier, J.: A synchronized dating of three Greenland ice
cores throughout the Holocene, *Journal of Geophysical Research Atmospheres*, 111, 1–11, <https://doi.org/10.1029/2005JD006921>, 2006.
- Vinther, B. M., Buchardt, S. L., Clausen, H. B., Dahl-Jensen, D., Johnsen, S. J., Fisher, D. A., Koerner, R. M., Raynaud, D., Lipenkov, V.,
Andersen, K. K., Blunier, T., Rasmussen, S. O., Steffensen, J. P., and Svensson, A. M.: Holocene thinning of the Greenland ice sheet,
Nature, 461, 385–388, <https://doi.org/10.1038/nature08355>, 2009.
- 615 Weikusat, C., Kipfstuhl, S., and Weikusat, I.: Raman tomography of natural air hydrates, *Journal of Glaciology*, 61, 923–930,
<https://doi.org/10.3189/2015JoG15J009>, 2015.
- Weikusat, I., Westhoff, J., Kipfstuhl, S., and Jansen, D.: Visual stratigraphy of the EastGRIP ice core (14 m - 2021 m depth, drilling period
2017-2019), <https://doi.org/10.1594/PANGAEA.925014>, 2020.
- Weinhart, A. H., Kipfstuhl, S., Hörhold, M., Eisen, O., and Freitag, J.: Spatial Distribution of Crusts in Antarctic and Greenland Snowpacks
620 and Implications for Snow and Firn Studies, *Frontiers in Earth Science*, 9, 1–16, <https://doi.org/10.3389/feart.2021.630070>, 2021.
- Westhoff, J., Stoll, N., Franke, S., Weikusat, I., Bons, P., Kerch, J., Jansen, D., Kipfstuhl, S., and Dahl-Jensen, D.: A Stratigraphy Based
Method for Reconstructing Ice Core Orientation, *Annals of Glaciology*, pp. 1–12, <https://doi.org/doi.org/10.1017/aog.2020.76>, 2020.
- Winski, D., Osterberg, E., Kreutz, K., Wake, C., Ferris, D., Campbell, S., Baum, M., Bailey, A., Birkel, S., Introne, D., and Handley, M.:
A 400-Year Ice Core Melt Layer Record of Summertime Warming in the Alaska Range, *Journal of Geophysical Research: Atmospheres*,
625 123, 3594–3611, <https://doi.org/10.1002/2017JD027539>, 2018.